How to cite: Angew. Chem. Int. Ed. 2024, e202416543
doi.org/10.1002/anie.202416543

Catalysis by Cavitation Bubbles on CuO

Localized Oxidative Catalytic Reactions Triggered by Cavitation Bubbles Confinement on Copper Oxide Microstructured Particles.

*Valarmathi Mahendran[+], Quang Thang Trinh[+], Xie Zhangyue, Umesh Jonnalagadda, Tim Gould, Nam-Trung Nguyen, James Kwan, Tej S. Choksi, Wen Liu, Sabine Valange, François Jérôme, and Prince Nana Amaniampong**

Abstract: Efficient energy transfer management in catalytic processes is crucial for overcoming activation energy barriers while minimizing costs and CO_2 emissions. We exploit here a concept of CuO particle design with multiple gas-stabilizing sites, engineered to function as cavitation nuclei and catalysts. This concept facilitates the selective and efficient acoustic energy transfer directly to the catalyst surface, avoiding the undesired dissipation of acoustic energy into the bulk solution while demonstrating superior cavitation properties at lower acoustic pressure amplitudes. Utilizing a chemical thermometric approach, we demonstrate that the local temperature on the surface of our CuO particles during cavitation bubble implosions can create an effective equivalent temperature of about 360 °C. This temperature effect facilitates the efficient catalysis of oxidative reactions using an organic pollutant probe molecule. Density functional theory (DFT) calculations were used to assess the decomposition of H_2O_2 and of pollutant probe molecule on CuO (111). Our work represents a significant advance in sonocatalytic systems, promising efficient energy use in catalytic reactions.

[*] V. Mahendran,[+] Prof. S. Valange, Dr. F. Jérôme, Dr. P. N. Amaniampong
CNRS, Université de Poitiers, Institut de Chimie des Milieux et Matériaux de Poitiers (IC2MP)
(ENSI-Poitiers), B1, 1 rue Marcel Doré, 86073 Poitiers, France
E-mail: prince.nana.amaniampong@univ-poitiers.fr

Dr. Q. T. Trinh,[+] Prof. T. Gould, Prof. N.-T. Nguyen
Queensland Micro and Nanotechnology Centre, Griffith University, Nathan, Queensland, 4111, Australia.

X. Zhangyue, Dr. U. Jonnalagadda, Prof. T. S. Choksi, Prof. W. Liu
School of Chemistry, Chemical Engineering and Biotechnology, Nanyang Technological University, 62 Nanyang Drive,Singapore, Singapore 637459

Prof. J. Kwan
Department of Engineering Sciences, University of Oxford, Parks Rd, Oxford OX1 3PJ, UK

[+] V.M is credited for the experiments and Q.T.T is credited for the computational results.

Introduction

Managing energy transfer in catalytic processes is crucial not only for efficiently overcoming activation energy barriers but also for reducing overall operational costs and CO_2 emissions.[1] Traditionally, catalytic processes rely on fossil fuels as their energy source. However, the shift towards "defossilization" necessitates a deeper understanding of how alternative, sustainable energy sources can be efficiently transferred to catalysts.[1d] Electrocatalysis and photocatalysis are among the most extensively studied methods in this regard.[2] Numerous studies have demonstrated how catalysts can efficiently harness electricity or photons to drive chemical reactions. Electromagnetic induction heating is another emerging strategy.[3] This technique allows for the specific heating of the surface of a heterogeneous catalyst, thereby minimizing inefficient energy transfer and heat dissipation issues commonly encountered in catalysis. In addition to these technologies, ultrasound is experiencing a resurgence.[4] Piezoelectric materials, when electrified, can generate ultrasonic waves that propagate through liquids.[5] At high acoustic energy levels, these waves create cavitation bubbles. The rapid compression and decompression cycles within these bubbles lead to extreme temperatures (> 1000 K) and pressures (> 100 bar).[4a,6] Upon collapse, the cavitation bubbles release stored acoustic energy locally, a phenomenon observable as sonoluminescence.[7] The potential to selectively confine these cavitation events to the surface of a heterogeneous catalyst is highly intriguing, as it offers a method for efficient acoustic energy transfer to catalytic surfaces. However, achieving this selective confinement remains a significant scientific challenge, which we partly address in this report.

Previous studies have demonstrated that the addition of solid particles during ultrasonic irradiation of a liquid can serve as nuclei for the formation of cavitation bubbles.[8] The presence of trapped gas pockets on the surface of these particles facilitates the nucleation of cavitation bubbles. Once formed, these bubbles detach from the particle surface and implode into the solution. This principle of heterogeneous cavitation has been primarily used to reduce the energy consumption in sonochemical reactions.[9] However, the application of this principle in catalysis presents a more complex challenge. In catalytic systems, the solid catalyst surface must not only initiate the nucleation of cavitation bubbles but also prevent their unwanted diffusion and

implosion in the liquid phase, which would result in inefficient energy transfer due to dissipation in the bulk solution. In current sonocatalytic systems, solid catalytic materials are not optimized to fully harness the heat and radicals generated in situ during bubble implosion. This inefficiency arises because bubble implosions typically occur at a spatial distance from the solid catalytic materials, limiting the interaction between the catalysts and the heat or reactive species produced, Scheme 1.

To address this challenge, we drew inspiration from the work of Fu et al.[10] on the synthesis of polymeric golf-ball-like microparticles, as well as our prior research on the synthesis of CuO particles as cavitation agents.[11] We discovered here that CuO particles, with their multiple gas-stabilizing sites can, not only serve as nuclei for the formation and growth of cavitation bubbles but also help sustain these bubbles on their surface. This fine control of the nuclei and fate of cavitation bubbles allowed us to selectively and efficiently transfer the acoustic energy onto the CuO suface which is concommittanly served as a heterogeneous catalyst. This strategy opens a path to selectively heat the surface of the CuO catalyst, thus avoiding heating of the whole solution as usually observed with conventional catalytic reactions. To demonstrate the feasibility of this concept, we investigated the CuO catalytic decomposition of H_2O_2 as a probe reaction, which provided us a means to assess the proximity of cavitation bubbles to the CuO catalytic surface in situ, and thus the local transfer of the acoustic energy.

Results and Discussions

CuO Preparation and Characterization

Catalytic surfaces of CuO engineered multicavities were typically prepared using polystyrene beads as sacrificial templates, a catalyst design referred herein as CuO-MC (**Figure S1**). The detailed synthesis procedure for these engineered CuO-MC catalysts was very recently reported by our groups[11] and is described in the Methods section, ′CuO Catalyst Synthesis.′ To highlight the contribution of multi-cavities to confine cavitation bubbles on the CuO-MC catalytic surface, a CuO catalytic material with no multi-cavities, and hereafter called CuO-DS, with DS meaning dense sphere, was also prepared (detailed synthesis protocol of CuO-MC and CuO-DS are described in the Methods section of the Supporting Information). A thorough characterization of the freshly prepared CuO-MC catalyst was first conducted, employing a range of complementary techniques, including X-ray diffraction (XRD), scanning electron microscopy (SEM), and X-ray photoelectron spectroscopy (XPS). The XRD patterns, Figure 1, revealed predominant peaks at $2\theta = 35.4°$ and 38.7°, which were unequivocally identified as the CuO [−1 1 1] and CuO [1 1 1] reflections, indicative of the high purity of the monoclinic CuO phase.[8a,12] These characterizations corroborate the successful synthesis of CuO-MC. SEM imaging provides further insights into the catalyst‘s morphology, Figure 1b. As indicated in Figure 1b, the design of CuO spheres bearing surface multicavities was experimentally realized. The average size of the synthesized CuO-MC catalyst was determined to fall within the range of 3 to 5 μm, accompanied by surface cavities with dimensions in the range from 300 to 400 nm, Figure 1b insert. The XPS analysis of the as-prepared CuO-MC cavitation agent

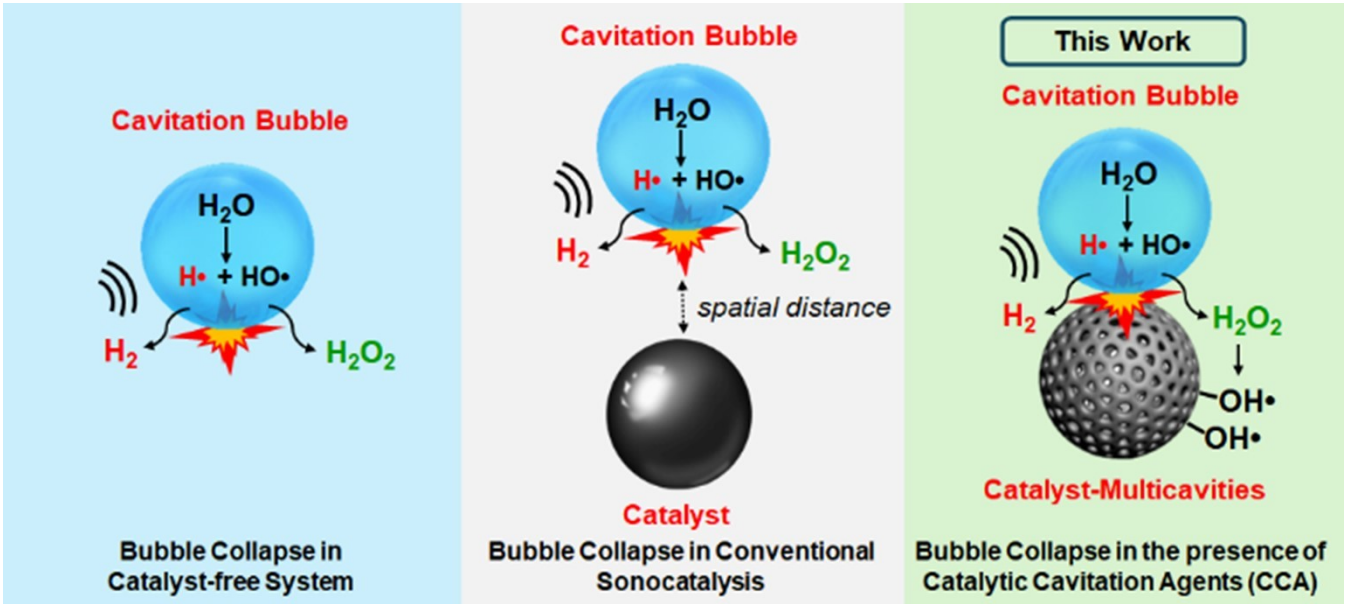

Scheme 1. Cavitation bubble collapse in; catalyst-free, conventional sonocatalysis and catalytic cavitation agent systems (this work).

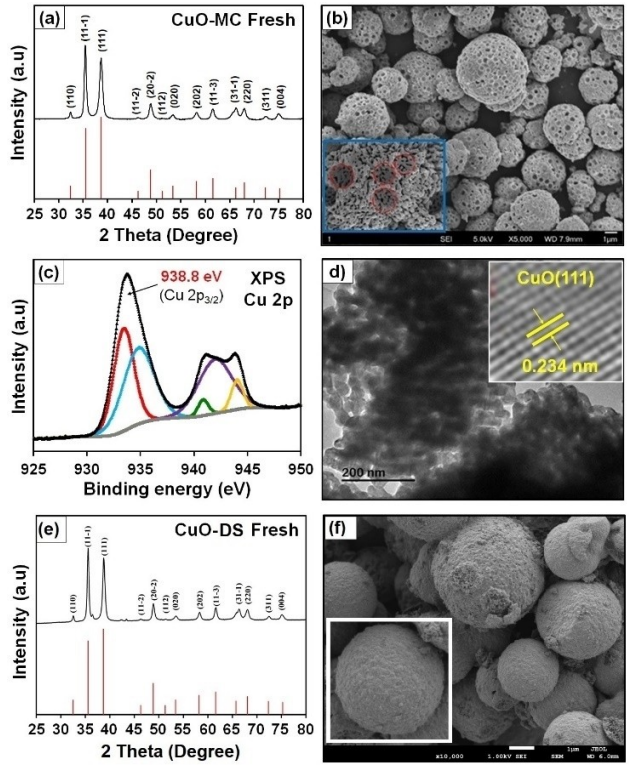

Figure 1. (a) XRD of as-prepared CuO-MC, (b) SEM images of CuO-MC, (c) Cu2p XPS analysis, (d) TEM analysis of as-prepared CuO-MC catalyst with HR-TEM insert, (e) XRD of as-prepared CuO-DS, (f) SEM images of CuO-DS.

furnished additional evidence confirming the composition of catalyst surface.

The observed binding energy centered at 933.8 eV, which aligns with the core level of Cu $2p_{3/2}$, unambiguiously establishes the formation of Cu^{2+} species in CuO-MC, Figure 1c.[13] The additional peaks at 941 and 943 eV are attributed to the shakeup satellites. Examination of the Cu LMM spectra revealed a prominent peak with a binding energy centered at 917.8 eV, **Figure S2, SI**,[13b,14] a distinctive feature indicative of CuO material. Cu-containing phases with any other oxidation state, e. g. Cu_2O, was not detected by any characterization. The as-prepared CuO-MC particles exhibited a BET surface area of 12 m^2/g. TEM analysis, Figure 1d, confirms the homogeneous distribution of the CuO-MC particles, while the HRTEM image, Figure 1d insert, reveals well-defined CuO (111) lattice fringes with an interplanar spacing of 0.234 nm.[15]

For comparison, XRD (Figure 1e) and SEM (Figure 1f) characterizations of CuO-DS were also conducted. The XRD patterns displayed prominent peaks at $2\theta = 35.6°$ and 38.7°, which were clearly identified as the CuO [−1 1 1] and CuO [1 1 1] reflections. Notably, a Cu_2O phase, accounting for 4 % of the total CuO formation, was also observed at $2\theta = 36.4°$ and 42.4°. The dense spherical morphology was confirmed through SEM analysis, revealing an average particle size bewteen of 3 to 5 µm, comparable to that of CuO-MC.

Catalytic Cavitation Agents. To explore the local confinement of cavitation bubbles on the CuO-MC catalytic surface, we first evaluated the acoustic response of CuO-MC, focusing on its ability to nucleate inertial cavitation at lower pressure amplitudes in accordance with the concept of heterogeneous cavitation. Results were then compared with the CuO DS catalyst to emphasize the role of multicavities in ehancing cavitation performance.

In line with our previous work,[11] Figure 2a reveals that the CuO-MC catalyst exhibited a cavitation threshold at a notably lower pressure amplitude of 1.73 MPa. In contrast, the reference CuO-DS displayed significantly less efficient cavitation across a broader pressure range of 0.8 to 4.23 MPa. Pure water, which generally requires a substantially higher-pressure amplitude of 140 MPa to induce cavitation,[16] did not cavitate at all under the tested conditions. As expected, the enhancement in cavitation response at lower pressure amplitude exhibited by the CuO-MC supports the key role of multicavities to stabilize gas bubbles, which significantly reduces the energy requirement (details of the energy estimation are provided in **S3, SI**) for inertial cavitation. In addition to examining the acoustic response profile, we validated the frequency content both above and at the cavitation thresholds for the synthesized CuO-MC catalyst, Figure 2b(i). Here, prominent broadband noise was observed at and above the cavitation threshold, which are indicative of inertial cavitation. In other words, the presence of CuO multicavities during sonolysis not only enhance the acoustic response but also promotes inertial cavitation. Meanwhile, the analysis with CuO-DS, Figure 2b-(ii), and in neat water, Figure 2b(iii), did not show any significant broadband noise. The duration for which the CuO catalysts maintain their cavitation response is crucial, as it reflects the period during which the CuO catalysts remain functional under continuous irradiation. To investigate this further in Figure 2c, we examined the duration of cavitation in the presence of CuO catalyst (CuO-MC and CuO-DS) and pure water over a 10-min period of irradiation at a 33 % duty cycle in the presence of argon-oxygen gas (50:50) mixtures. Our findings demonstrated a consistent cavitation response in the presence of CuO-MC over the 10-min irradiation period. In contrast, sporadic acoustic intensity was observed in the presence of pure water and CuO-DS. These results indicate once again that CuO-MC catalyst acts as a nucleation site for sustained cavitation formation, whereas in pure water, the stochastic and random nature of cavitation events leads to sporadic acoustic intensity. Collectively, these findings strongly confirm the capacity of CuO-MC catalysts with engineered surface nano-cavities to act as a proficient nucleating agent.

To highlight the efficiency of CuO MC in promoting inertial cavitation, we next analyze the ultrasonic solution by means of Electron Paramagnetic Resonance (EPR) spectroscopy and using DMPO as a radical scavenger to assess the formation of $^{\bullet}OH$ stemming from water sonolysis, Figure 3. During the ultrasonication of neat water with a saturated Ar/O_2 (50:50) gas mixture, i. e. in the absence of CuO (MC or DS), no signal was observed at 10 % duty cycle indicating the absence of cavitation in neat water under the acoustic

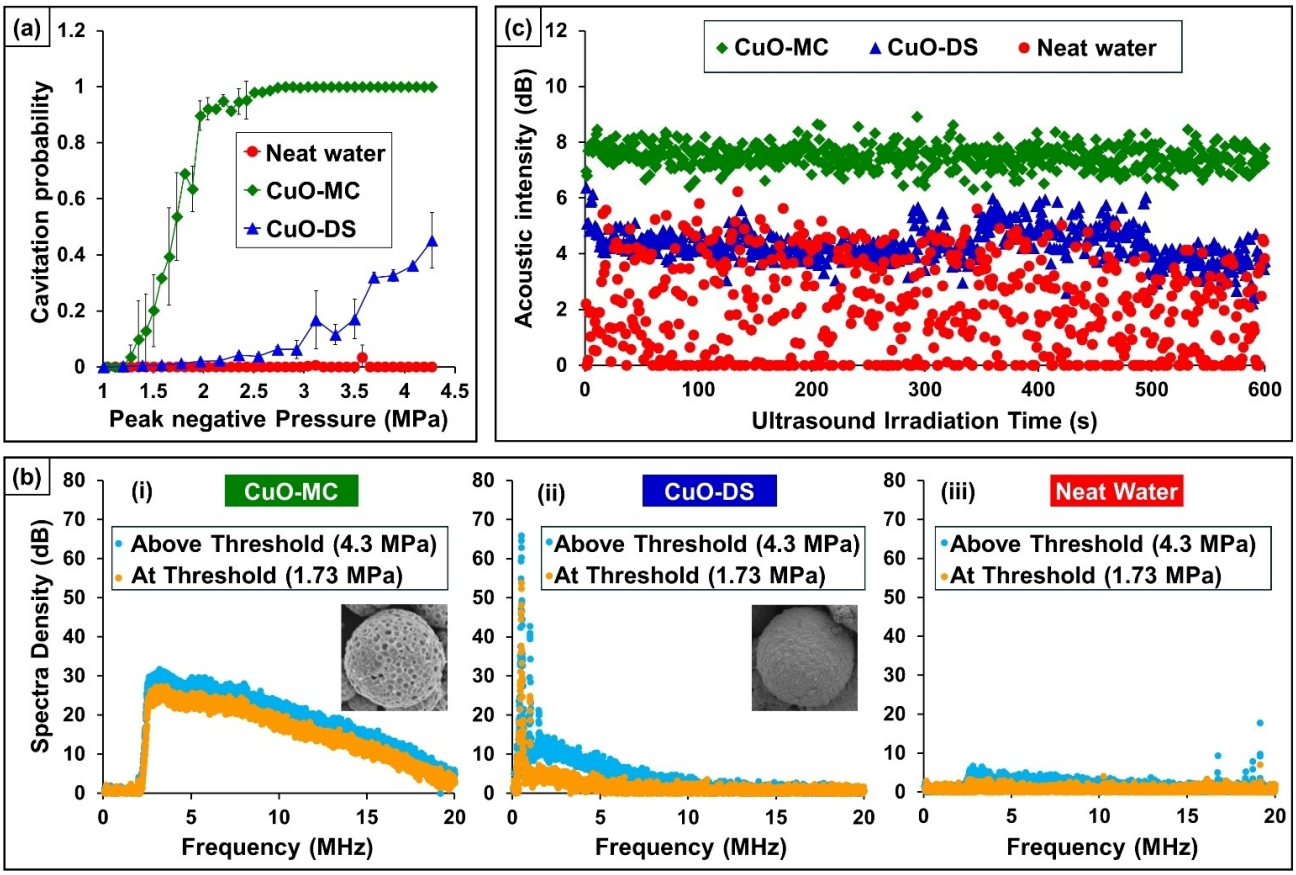

Figure 2. (a) Cavitation potential of CuO-MC, CuO-DS and neat water at various acoustic pressures, (b) visualization of acoustic response of CuO-MC, CuO-DS particles and neat water by assessing the acoustic cavitation intensity vs time. Power spectral density was further analyzed to validate the quality of noise. The power spectral density curve expressed greater evidence of broadband cavitation in the presence of CuO-MC (b) than in the presence of CuO-DS (b(ii)) and neat water (b(iii)).

pressure regime investigated. In contrast, in the presence of CuO MC cavitation agents, characteristic quadruplet peaks corresponding to DMPO-•OH were detected. These peaks indicate that CuO-MC can effectively nucleate cavitation bubbles, thereby enhancing the generation of reactive oxygen species (ROS). In contrast, when sonication was performed with CuO-DS, EPR measurements exhibited significantly lower signal intensities of DMPO-•OH, Figure 3. This result clearly demonstrates that CuO-DS are not effective cavitation agents and thus have limited efficiency in enhancing inertial cavitation.

In situ assessment of the proximity between cavitation bubbles and CuO-MC. To in situ assess the proximity of cavitation bubbles with the surface of CuO catalyst, we investigated the catalytic decomposition of H_2O_2 as a probe reaction. Indeed, during ultrasonic irradiation, water vapors trapped within (or in the periphery of) the cavitation bubbles are cleaved resulting in the production of •OH and •H radicals. These radical species subsequently recombine to form H_2O_2 and H_2, respectively. CuO has the ability to catalytically decompose H_2O_2, as gleaned from Density Functional Theory (DFT) investigations which is discussed later in this paper. We thus hypothesized that monitoring the abatment of H_2O_2 during ultrasonic irradiation in the presence of CuO would reflect the proximity between CuO particles and cavitation bubbles.

First, we assessed the production rate of H_2O_2 during ultrasonic irradiation of neat water (i. e. without any CuO). This will serve as a reference reaction to assess the interaction of CuO with cavitation bubbles. In this study, a cup-horn high-frequency (496 kHz) ultrasound reactor was employed. The bulk liquid temperature of the reactor was regulated using an external chilling system. The reactor operated at a full working amplitude (100 %) in continuous mode, sufficient to induce cavitation in pure water. The formation of H_2O_2 was tracked using a standardized spectrophotochemical method. After 60 min of irradiation, ~0.85×10^{-3} mol/L of H_2O_2 were observed for sonolysis performed under argon atmosphere (production rate of 2.28×10^{-7} mol/Ls), ~1.5×10^{-3} mol/L for oxygen atmosphere (production rate of 4×10^{-7} mol/Ls), and ~5.1×10^{-3} mol/L for the argon/oxygen gas mixture (production rate of 1.39×10^{-6} mol/Ls). These measurements were taken at gas flow rates of 10 mL/min, Figure 4a. Based on the obtained H_2O_2 concentrations, the argon/oxygen gas mixture appears to be the most profilic at facilitating H_2O_2 formation and was chosen for all subsequent sono-catalytic experiments, unless specified otherwise.

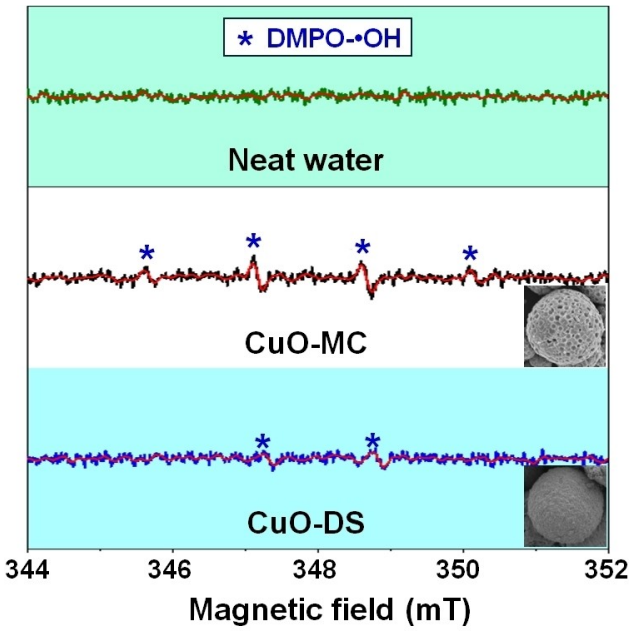

Figure 3. Measured EPR spectra obtained in the presence of (i) CuO-MC and (ii) CuO-DS. All spectra were collected under argon/oxygen gas mixture (50%/50%) with ultrasound irradiation under 4.3 MPa pressure amplitude for 20 min in DI water. Analysis conditions: 25 mM DMPO, 10% duty cycle, 1 mg/mL catalyst, 500 kHz ultrasound frequency. Inserted figures are SEM images of CuO-MC and CuO-DS, respectively. Asterisks show characteristic signals of DMPO-•OH.

Next, to demonstrate the ability of CuO to catalytically decompose H_2O_2, CuO-MC and CuO-DS were both suspended in an aqueous solution of H_2O_2 (5 mmol) at 30 °C for 60 min under silent conditions, Figure 4b. CuO-MC and CuO-DS catalyzed the decomposition of H_2O_2 at a similar rate (~10×10^{-8} mol/Ls). We next investigated the impact of cavitation on CuO-MC and CuO-DS on H_2O_2 formation from sonolysis. After 60 min of irradiation, Figure 4c, the acumulated concentration of H_2O_2 was found to be only 0.6×10^{-3} mol/L in the presence of CuO-MC. This was a remarkable 88% reduction from the concentration observed (5.1×10^{-3} mol/L) in neat water without any CuO-MC catalyst. This significant suppression of H_2O_2 formation within the bulk liquid phase indicates enhanced in situ decomposition of H_2O_2 near the CuO-MC surface. These interactions effectively restrict the accumulation of H_2O_2 in the bulk liquid phase. To substantiate the interaction of the CuO-MC particles surface with cavitation bubbles and its consequential H_2O_2 in situ decomposition, a hot filtration test was conducted after 60 min of irradiation in the presence of CuO-MC catalysts. In this test, the particles were separated from the solution via filtration. The filtered solution was subsequently irradiated by ultrasound, Figure 4d. This experiment revealed a notable increase in the formation of H_2O_2, reaching approximately 5.7×10^{-3} mol/L after 60 min of irradiation time, i.e. a similar H_2O_2 production rate observed in neat water. This strongly supports that CuO-MC catalyst efficiently interacts with cavitation bubbles leading to the in situ catalylic decomposition of H_2O_2 by CuO-MC, suppressing its accumulation in the bulk phase. To elucidate the significance of surface engineering, CuO-DS (dense spheres) was also tested as a benchmark. While CuO-DS exhibited no difference in H_2O_2 decomposition rate compared to CuO-MC under silent conditions, Figure 4b, its rate of H_2O_2 decomposition lagged significantly behind CuO-MC under ultrasonic irradiation. Analysis revealed a measured H_2O_2 concentration of 3.8×10^{-3} mol/L after 60 mins of irradiation. Interestingly, sonolysis in the presence of CuO-DS represented only a ~20% reduction in H_2O_2 generation compared to that observed in pure water without any catalyst. This observation confirms that the presence of multicavities on the CuO particles is crucial for confining cavitation events on its surface, opening a great means to selectively transfer the acoustic energy and reactive oxygen species to the CuO surface.

Our experimental observations for CuO catalytic decomposition of H_2O_2 were supported computationally through Density Functional Theory (DFT) calculations. All the DFT calculations are performed using the VASP package.[17] To study the trend of H_2O_2 activation, only electronic energies are used and the findings are summarized in Figure 5 and more detailed analysis is presented in **S5, SI**. In vacuum, H_2O_2 adsorbs on the clean CuO (111) surface with an adsorption energy of −68 kJ/mol, **Figure S4, SI**. Two activation pathways for H_2O_2 on CuO are identified: O–O bond scission to form two •OH fragments with an activation barrier of 22 kJ/mol, Figure 5b, and O–H bond dissociation to form •H and •OOH fragments with a lower activation barrier of 7 kJ/mol, Figure 5c. Although the O–H dissociation pathway is 15 kJ/mol kinetically more feasible, it is less energetically favorable compared to the O–O scission pathway. These trends are consistent with findings by Guo et al.[18] and Lousada et al.[19]

In the aqueous phase, H_2O_2 shows stronger adsorption than in the gas phase with an adsorption energy of −154 kJ/mol, **Figure S5 and S6 (SI)**. This stronger adsorption energy is possibly due to the synergy of the H-bonds to strengthen the adsorption of H_2O_2, as was reported by Michel et al.[20] The activation barrier for the •OH pathway in water increases slightly to 38 kJ/mol, Figure 5d, still feasible under our experimental conditions. However, the •OOH pathway is significantly inhibited in water with a high activation barrier of 104 kJ/mol because the H-OOH bond in H_2O_2 is stabilized by hydrogen bonding with surrounding water molecules, Figure 5e. Importantly, the •OOH pathway is even less energetically favorable than the competitive •OH pathway in an aqueous environment, Figure 5a. Thus, in the micro-solvation environment that resembles the aqueous phase, H_2O_2 decomposition on CuO predominantly occurs through the HO-OH cleavage pathway, efficiently generating OH* species adsorbed on the CuO surface. Two OH* species eventually could combine to produce H_2O and atomic O (finally forming O_2), as was reported in Guo et al.[18] The stable structural integrity of CuO-MC under ultrasonic conditions, as shown in **Figure S3, SI**, supports the preference for the •OH pathway. This is because the activation of H_2O_2 via the •OH pathway does not alter the

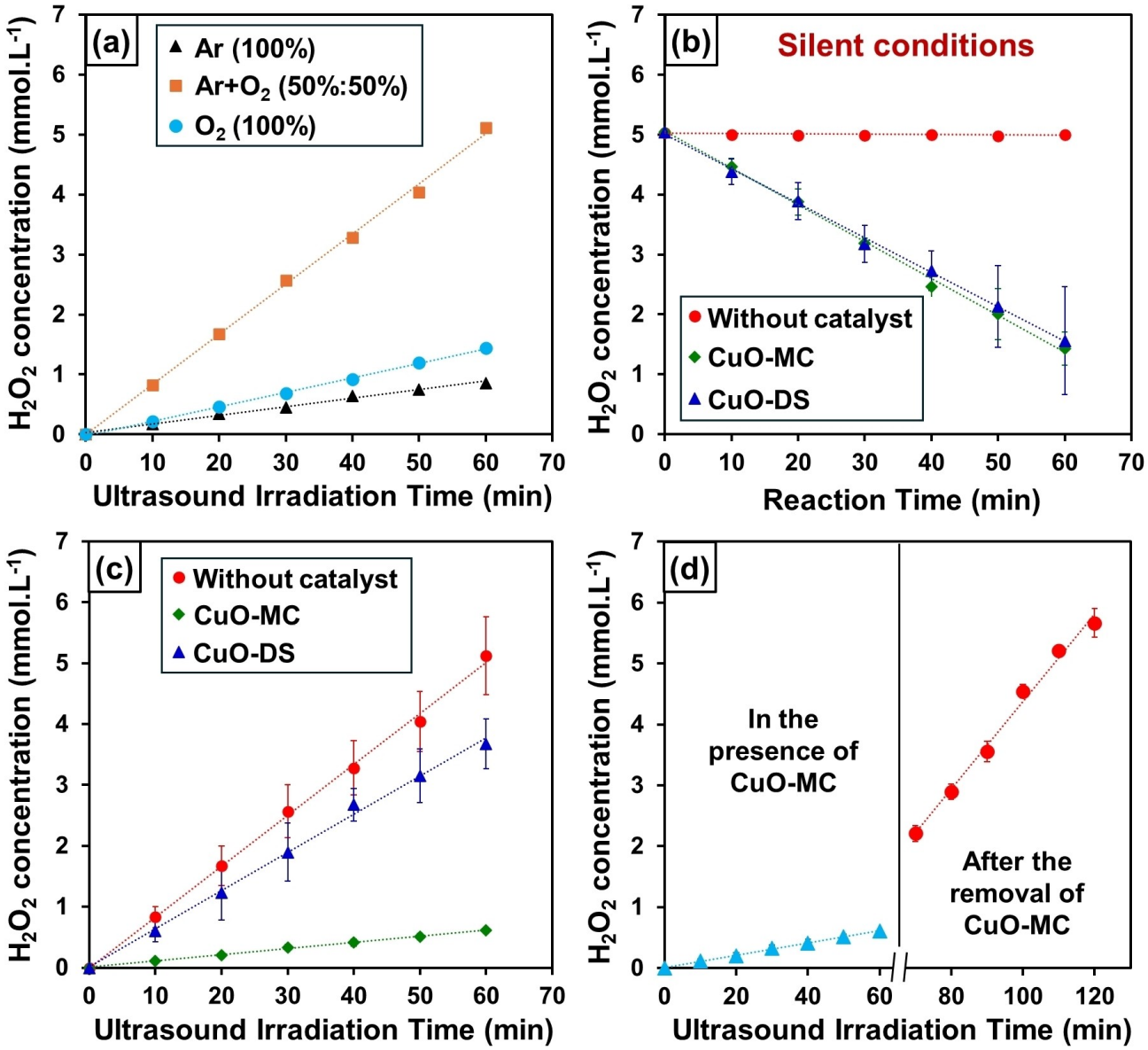

Figure 4. (a) Quantification of hydrogen peroxide formation under different gas atmosphere; Reaction conditions: 100% acoustic amplitude, 25 °C bulk liquid temperature, 10 mL gas flow rate (O_2/Ar: 50%-50), 496 kHz ultrasound frequency, (b) Hydrogen peroxide decomposition in the presence of CuO-MC, CuO-DS and solid-free conditions in silent conditions. Reaction conditions: 5 mmol of H_2O_2, 30 °C bulk temperature, 60 min of reaction time. (c) Quantification of hydrogen peroxide formation under catalytic cavitation agent (CuO-MC) and CuO-DS, Reaction conditions: 100% acoustic amplitude, 25 °C bulk liquid temperature, 10 mL gas flow rate (O_2/Ar: 50%-50), 496 kHz ultrasound frequency (d) hot filtration test and quantification of hydrogen peroxide formation, Reaction conditions: 100% acoustic amplitude, 25 °C bulk liquid temperature, 10 mL gas flow rate (O_2/Ar: 50%-50), 496 kHz ultrasound frequency. All error bars were plotted based on tripicate experiments.

CuO structure over time (as seen in the XRD analysis of the spent CuO-MC in **Figure S3, SI**).[8a,21] In contrast, activation of H_2O_2 via the •OOH pathway generates •H atoms that adsorb on the surface lattice oxygen of CuO, causing significant reduction in the CuO structure, as seen in our previous studies.[15,21a,22]

In situ assessment of local temperature on CuO-MC via chemical thermometry. Next, we conducted an experimental investigation to assess the effective local temperature (T_{eff}) released on the CuO-MC surface at the cavitation bubble collapse time. This was achieved through chemical thermometry, using the oxidative degradation of methyl orange (MO) as a probe reaction. First, the oxidative degradation of MO was studied under silent conditions. To this end, 25 mg of the CuO MC was suspended in 19 mL of an aqueous solution containing 50 ppm of MO. Then, H_2O_2 (10.2 µL) was added stepwise at a similar concentration (~5×10^{-3} mol/L) it was produced during sonolysis of water to be as close as possible to the ultrasonic conditions, i.e. at an addition rate of 1.39×10^{-6} mol/Ls. To monitor the oxidative degradation process, aliquots (100 µL) were with-

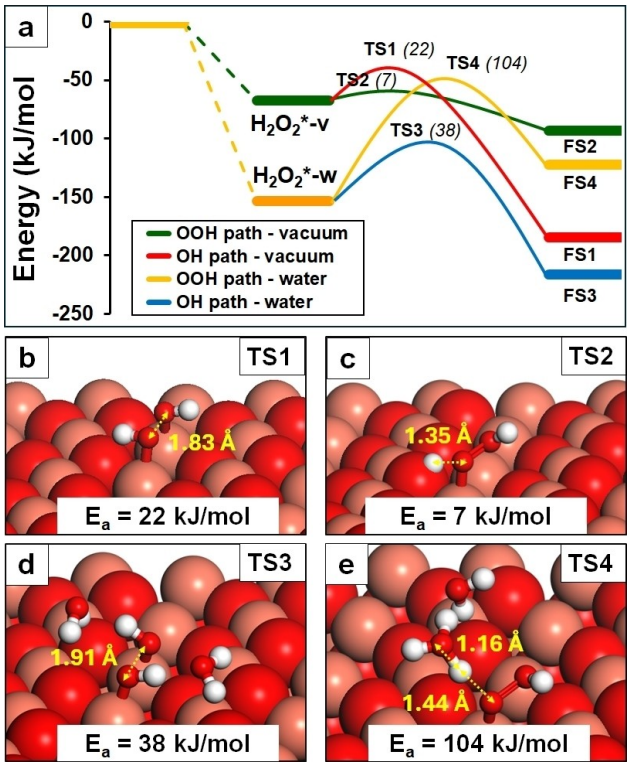

Figure 5. (a) Electronic energy profile for H_2O_2 decomposition on CuO (111) surface in vacuum and in a micro-solvation environment. H_2O_2*-v and H_2O_2*-w indicate adsorbed H_2O_2 in vacuum and in water, respectively. Transition states of H_2O_2 activation in vacuum conditions via (b) OH pathway (TS1) and (c) OOH pathway (TS2). Transition states of H_2O_2 activation in aqueous conditions via (d) OH pathway (TS3) and (e) OOH pathway (TS4).

drawn at specific intervals and subjected to analysis using UV/Vis spectroscopy.

By analyzing the kinetics of MO degradation at various temperatures ranging from 30 °C to 100 °C, it was observed that the reaction rates logically increased with temperature (from 13×10^{-3} ppm/s at 30 °C to 36×10^{-3} ppm/s at 100 °C), which is consistent with literature reports showing that the MO degradation process is endothermic, **Figure S7, SI**. An Arrhenius plot of *ln*(k) versus 1/T, Figure 6a, yielded a straight line, from which the effective local temperatures (T_{eff}) on the surfaces of CuO-MC was estimated, as detailed later in the manuscript. To determine the effective local temperature (T_{eff}) on the CuO-MC surface during bubble implosions, MO degradation reactions were conducted under the same conditions (25 mg of CuO-MC suspended in 20 mL solution of MO (50 ppm), continuous gas flow (Ar/O_2, 50/50 % gas mixtures) at a flow rate of 10 mL/min, with the bulk reaction temperature maintained at 25 °C), but in the presence of ultrasound (496 kHz). The effective local temperature (T_{eff}) on the CuO-MC surface was tentatively calculated from the Arrhenius expression using the activation parameters obtained in Figure 6a. By using the Arrhenius expression in Figure 6a, we could roughly estimate the effective local temperature (T_{eff}) on the CuO-MC surface upon bubble implosion to be around 360 °C.

A control experiment, Figure 6b, was conducted using neat water devoid of catalytic cavitation agents. The degradation rate of methyl orange (MO) was measured at 59×10^{-3} ppm/sec. However, the introduction of CuO-MC under identical experimental conditions resulted in a significantly enhanced MO degradation rate of 221.6×10^{-3} ppm/sec. This represents a substantial 276 % increase in the degradation rate compared to the control experiment, Figure 6b. The enhanced MO degradation rate is attributed to the in situ activation of the CuO-MC catalytic surface by the (i) the transfer of acoustic energy to the catalyst surface, and (ii) an increased flux of reactive radicals. For comparative analysis, experiments were also performed using CuO-DS as the catalytic agent. The MO degradation rate observed with CuO-DS was 89.4×10^{-3} ppm/sec, indicating only 50.8 % increase in the degradation rate relative to the control. These results clearly demonstrate the superior catalytic efficiency of CuO-MC in enhancing the degradation rate of MO through cavitation.

CuO-MC assisted catalytic reactions and computational investigations. To further explore the catalytic ability of our engineered CuO-MC, the amplitude of our ultrasound reactor was reduced from 100 % (0.26 WmL^{-1} acoustic power density) to 50 % (0.13 WmL^{-1} acoustic power density). Ideally, this reduction in amplitude should significantly lower cavitation generation and hence H_2O_2 formation (production rate of 2.9×10^{-7} mol/Ls *vs* 1.39×10^{-6} mol/Ls at 100 % amplitude in neat water) (**S8, SI**). Delightfully, CuO-MC enhanced the rate of MO degradation by 356.9 % compared to reactions in neat water under similar acoustic conditions, Figure 7a. While merely 40.5 % enhancement in MO degradation was achieved over CuO-DS. Next, the initial concentration of the MO substrate was increased by 900 %, from 50 ppm to 500 ppm, Figure 7b. Remarkably, even at reduced amplitude (50 %) after only 10 min of acoustic irradiation, we achieved a degradation of 60 % of the MO. Further extending the acoustic irradiation time to 60 min resulted in the near-complete degradation of MO. In contrast, the MO degradation experiment conducted with CuO-DS demonstrated significantly lower efficacy. After 10 min of acoustic irradiation, only 36 % of the MO was degraded, increasing to just 66 % after 60 min. Comparatively, in neat water (i. e., a catalyst-free system) subjected to ultrasound irradiation alone, only 22 % of MO was degraded after 10 min, reaching 50 % after 60 min. Once again, these results closely support the synergistic effect between cavitation bubbles and CuO MC.

DFT calculations were performed to elucidate the critical role of pre-adsorbed •OH species in the oxidative degradation of methyl orange (MO) on CuO. MO is used as a probe molecule to assess whether the CuO surface can assist in cleaving N=N bonds, the primary step for MO degradation. This step is followed by subsequent ring opening into smaller fragments.[23] Our DFT results indicate that the energy of the N=N bond in MO is approximately 420 kJ/mol (defragmenting MO into two smaller species). This high barrier implies that catalytic active sites may be necessary for N=N cleavage. On the pristine CuO (111) surface, MO adsorbs with a computed adsorption energy of −38 kJ/mol,

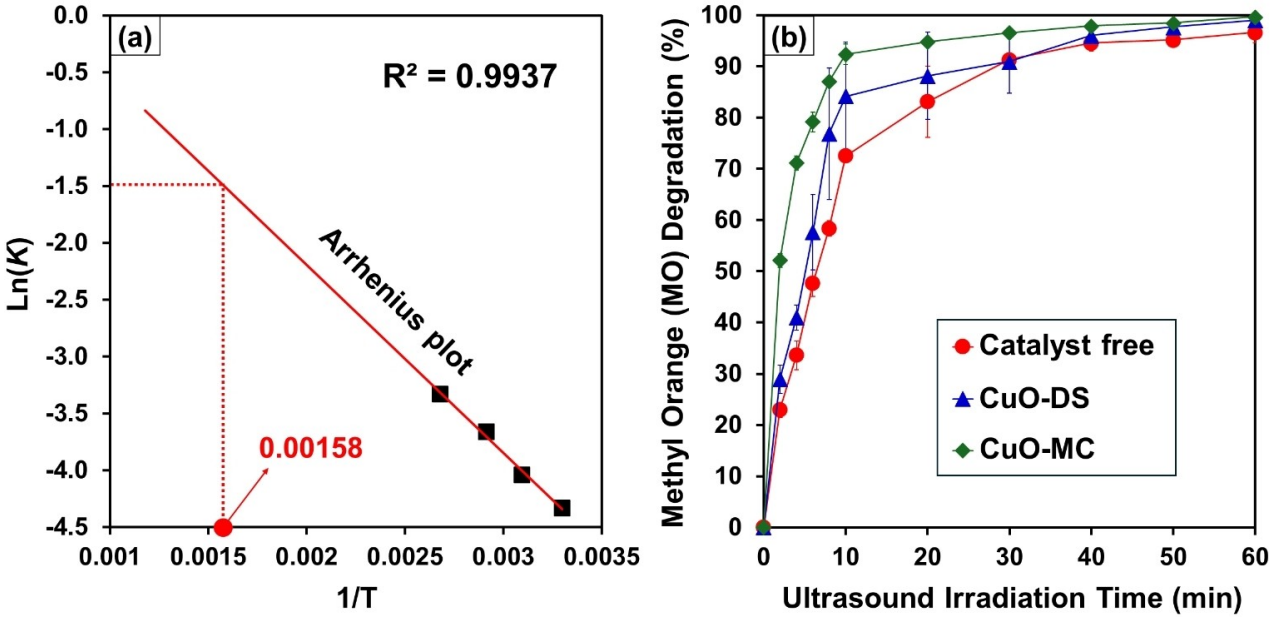

Figure 6. (a) Arrhenius plot of MO degradation in silent conditions. The rate constants were obtained by using a zero-order model. (b) Methyl orange degradation; substrate concentration = 50 ppm, acoustic amplitude = 100%, bulk liquid temperature = 25 °C, gas flow rate = 10 mL/min (O_2/Ar: 50%-50), ultrasound frequency = 496 kHz in the presence of CuO-MC, CuO-DS and catalyst-free condition.

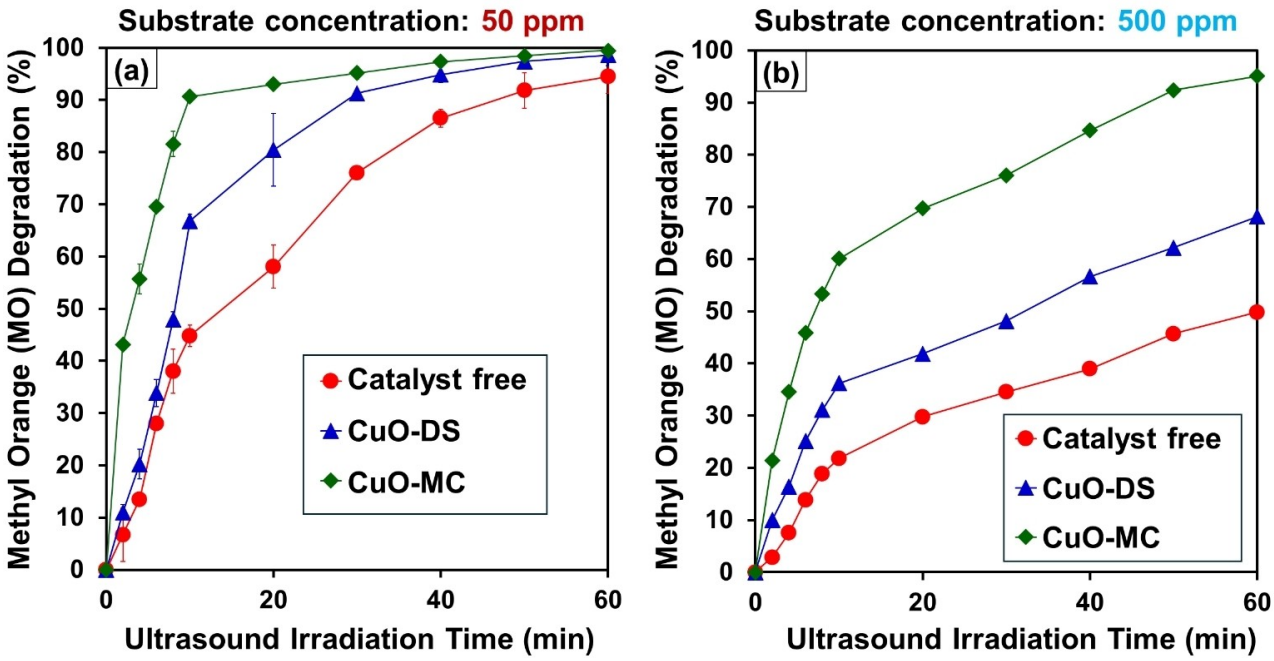

Figure 7. (a) Methyl orange degradation; substrate concentration = 50 ppm, acoustic amplitude = 50%, bulk liquid temperature = 25 °C, gas flow rate = 10 mL/min (O_2/Ar: 50%-50), ultrasound frequency = 496 kHz in the presence of CuO-MC, CuO-DS and catalyst-free condition. (b) Methyl orange degradation; substrate concentration = 500 ppm, acoustic amplitude = 50%, bulk liquid temperature = 25 °C, gas flow rate = 10 mL/min (O_2/Ar: 50%-50), ultrasound frequency = 496 kHz in the presence of CuO-MC, CuO-DS and catalyst-free condition. All error bars were plotted based on tripicate experiments. We would like to note that in all kinetic profiles we observed a change in the rate of reactions after 10 mins of ultrasound irradiation which might reflect issues of gas diffusion limitiations at higher ultrasound irradiation time.

Figure 8 and **Figure S9, SI**. The direct dissociation of the N=N bond on this surface faces a high activation barrier of 176 kJ/mol (TS1 in Figure 8). However, the N=N bond can be more readily cleaved if the nitrogen atoms are either reduced or oxidized, as indicated in prior studies.[23b,c,24]

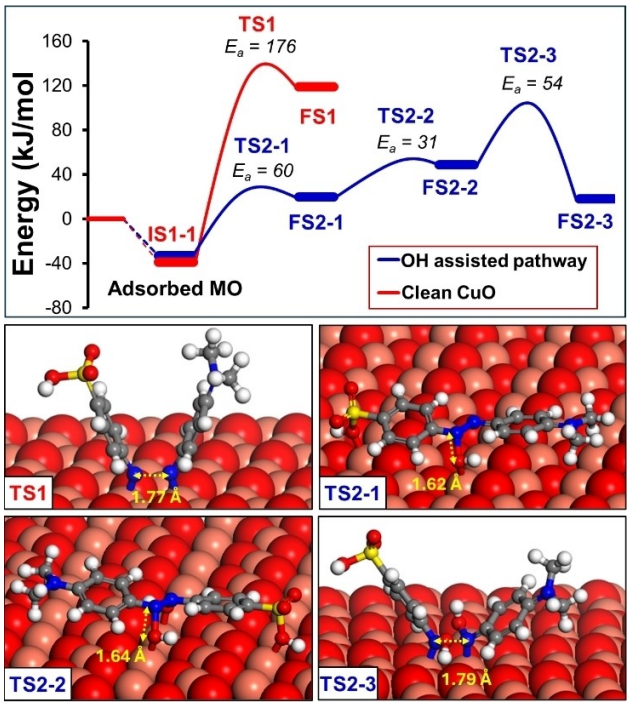

Figure 8. The potential energy profile and structures of transition states for the activation of methyl orange (MO) on CuO (111) (red) and OH* covered CuO (111) (blue). All the values are electronic enegies and computed without including contributions from solvation interactions.

Under high-frequency ultrasound conditions in our experiments, •OH species adsorb on the CuO surface,[8a,25] facilitating an alternative dissociation pathway for the N=N bond (illustrated in Figure 8 and **Figure S10, SI**). When MO adsorbs on the CuO (111) surface with two pre-adsorbed •OH groups (to oxidize two N atoms in MO), the computed adsorption energy is −33 kJ/mol, **Figure S9** (**SI**), comparable to the adsorption energy on clean CuO (111). The role of the two OH* species is to oxidize the two N atoms in MO. The computed barrier to oxidize the nitrogen atom in the benzenesulfonate fragment by surface OH* species is 60 kJ/mol (TS2-1 in Figure 8), lower than the 176 kJ/mol barrier for N=N bond dissociation on clean CuO (111). Following the oxidation of the first nitrogen atom, the second nitrogen atom in the dimethylamino phenyl fragment is also oxidized with a lower activation barrier of 31 kJ/mol, forming the diazenediol derivative (TS2-2 in Figure 8). The N–N cleavage in the diazenediol derivative requires an activation barrier of 54 kJ/mol, Figure 8. Thus, the OH* covered CuO (111) surfaces can plausibly dissociate the N=N bonds of MO.

Conclusion

A novel concept and disruptive catalytic approach, coined Catalytic Cavitation Agent (CCA), for assessing the impact of and synergistic interactions of cavitation bubbles on solid catalyst surfaces has been introduced. Results collected in this report shows that it was possible to selectively confine cavitation events on the surface of a metal oxide catalyst (CuO), by creating surface multicavities. These multicavities act as gas pockets not only to induce the nucleation of cavitation bubbles at a lower energy (1.34×10^{7} J) compared to 8.77×10^{10} J in neat water, but also to maintain those cavitation bubbles on the catalyst surface up to their implosion. This proximity of cavitation bubbles with catalytic surfaces led to synergistic effect (1) the acoustic energy accumulated within the cavitation bubbles is locally transferred to the catalytic surface, thus avoiding loss of energy by dissipation in the liquid phase, (2) cavitation bubbles provide the reactive oxygen species required for the catalytic degradation of pollutants and (3) the catalytic surface harnesses the heat and the reactive oxygen species created by the cavitation bubbles to speed up the degradation of MO (model pollutant) by a factor of about 276 %. All together, these results confirm that cavitation bubbles could be selectively confined on the surface of CuO MC where their implosion locally provides sufficient energy to induce the catalytic oxidative degradation of MO over CuO MC. Our experimental results, using methyl orange degradation as a probe reaction, demonstrate that an effective local temperature of about 360 °C can be achieved on the CCA surfaces upon bubble implosion. This pioneering approach in catalytic design paves the way for the development of advanced catalytic materials optimized for sonocatalysis, in particular for diverse applications such as chemical synthesis, environmental remediation, and water treatment. By harnessing the power of ultrasound, CCAs offer an energy-efficient alternative for catalytic reactions, operating at near-ambient bulk temperature. This innovative methodology opens new avenues for the design and application of catalytic materials, demonstrating the potential for significant advancements in sustainable and efficient catalysis. Our group is currently exploring the catalytic effects of other materials with similarly engineered surface structures.

Supporting Information. Methods description, extra characterization data for CuO-MC, spent CuO-MC, acoustic energy and acoustic intensity, extra data for methyl orange degradation and H_2O_2 calibration, detailed DFT investigation on H_2O_2 decomposition on CuO (111) and methyl orange adsorption and activation on CuO (111) surface.

Author Contributions

The manuscript was written through contributions of all authors. P.N. A, F. J and S. V supervised the experiments, V.M, X. Z and U. J performed the experiments, Q.T.T. performed the computational calculations, T. G, T.C and N–T. N supervised the computational work, W. L, T.C, P.N.A, F.J, J.K and S.V discussed and rationalized all experimental results in the manuscript. P.N.A wrote the manuscript, F.J, S.V, Q.T.T, T.C, W.L, J.K and P.N.A revised the manuscript, Q.T.T prepared all Figures in high resolution. Financial support was acquired by S.V. P.N.A., F.J. and W.L. All authors have given approval to the final version of the manuscript.

Acknowledgements

This project was financially supported by the ANR-NRF Joint Research Project SonoNanoCat jointly funded by the French National Research Agency (ANR reference: ANR-20-CE09-0030) and the Singapore National Research Foundation (NRF reference: NRF2020-NRF-ANR066), Prime Minister's Office. Dr Prince Nana Amaniampong acknowledges the financial support from the European Research Council (ERC) funded/Co-funded by the European Union (ERC, ConCASM, project agreement number 101117070). Views and opinions expressed are however those of the author(s) only and do not necessarily reflect those of the European Union or the European Research Council. Neither the European Union nor the granting authority can be held responsible for them. Valarmathi Mahendran, Dr. François Jérôme, Dr. Sabine Valange and Dr. Prince N. Amaniampong acknowledge financial support from the European Union (ERDF) and Région Nouvelle Aquitaine. This work also pertains to the French government program "Investissements d'Avenir" (EUR INTREE, reference ANR-18-EURE-0010). Tej S. Choksi acknowledges funding from a Ministry of Education Academic Research Fund Tier-1: RG87/23. Authors would like to thank Christine Canaff, Sandrine Arii, Julie Rousseau and Céline Boissard for the characterization experiments. Q.T.T and N.-T. N would like to acknowledge the financial support from the Australian Research Council (ARC) Laureate Fellowship (FL230100023). Q.T.T. and T.G. acknowledge the computational support from the Australian National Computing Initiative through NCMAS project sp13 and the Griffith University Gowonda HPC Cluster for the use of computational resources.

Conflict of Interest

Authors declare no competing interests.

Data Availability Statement

The data that support the findings of this study are available on request from the corresponding author. The data are not publicly available due to privacy or ethical restrictions.

Keywords: Catalytic cavitation agent · Localised heating · cavitation nucleation · Effective local temperature · Ultrasound irradiation

[1] a) F. Strieth-Kalthoff, M. J. James, M. Teders, L. Pitzer, F. Glorius, *Chem. Soc. Rev.* **2018**, *47*, 7190–7202; b) E. R. Welin, C. Le, D. M. Arias-Rotondo, J. K. McCusker, D. W. MacMillan, *Science* **2017**, *355*, 380–385; c) W. Wang, G. Tuci, C. Duong-Viet, Y. Liu, A. Rossin, L. Luconi, J.-M. Nhut, L. Nguyen-Dinh, C. Pham-Huu, G. Giambastiani, *ACS Catal.* **2019**, *9*, 7921–7935; d) T. K. Houlding, E. V. Rebrov, **2012**, 19-31.

[2] a) K. L. Skubi, T. R. Blum, T. P. Yoon, *Chem. Rev.* **2016**, *116*, 10035–10074; b) B. Seemala, A. J. Therrien, M. Lou, K. Li, J. P. Finzel, J. Qi, P. Nordlander, P. Christopher, *ACS Energy Lett.* **2019**, *4*, 1803–1809; c) U. Aslam, S. Chavez, S. Linic, *Nat. Nanotechnol.* **2017**, *12*, 1000–1005; d) A. Bauer, F. Westkämper, S. Grimme, T. Bach, *Nature* **2005**, *436*, 1139–1140; e) M. Marchini, G. Bergamini, P. G. Cozzi, P. Ceroni, V. Balzani, *Angew. Chem.* **2017**, *129* (42), 12996; f) F. Raimondi, G. G. Scherer, R. Kötz, A. Wokaun, *Angew. Chem. Int. Ed.* **2005**, *44*, 2190–2209; g) J. Wang, S. Dou, X. Wang, *Sci. Adv.* **2021**, *7*, eabf3989; h) C. Costentin, M. Robert, J.-M. Savéant, *Chem. Soc. Rev.* **2013**, *42*, 2423–2436; i) Y. Cai, J. Fu, Y. Zhou, Y.-C. Chang, Q. Min, J.-J. Zhu, Y. Lin, W. Zhu, *Nat. Commun.* **2021**, *12*, 586.

[3] a) Y.-Y. Yang, P. Zhang, N. Hadjichristidis, *J. Am. Chem. Soc.* **2023**, *145*, 12737–12744; b) C. Kerzig, X. Guo, O. S. Wenger, *J. Am. Chem. Soc.* **2019**, *141*, 2122–2127; c) Y. Qiu, W. J. Kong, J. Struwe, N. Sauermann, T. Rogge, A. Scheremetjew, L. Ackermann, *Angew. Chem. Int. Ed.* **2018**, *57*, 5828–5832.

[4] a) K. S. Suslick, *Science* **1990**, *247*, 1439–1445; b) K. S. Suslick, S. J. Doktycz, *J. Am. Chem. Soc.* **1989**, *111*, 2342–2344; c) K. S. Suslick, D. A. Hammerton, R. E. Cline, *J. Am. Chem. Soc.* **1986**, *108*, 5641–5642.

[5] a) G. Chatel, J. C. Colmenares, *Top. Curr. Chem.* **2017**, *375*, 8; b) H. Sudrajat, I. Rossetti, I. Carra, J. C. Colmenares, *Curr. Opin. Chem. Eng.* **2024**, *45*, 101043; c) H. Sudrajat, I. Rossetti, J. C. Colmenares, *J. Mater. Chem. A.* **2023**, *11*, 24566–24590.

[6] a) K. S. Suslick, *Sci. Am.* **1989**, *260*, 80–87; b) K. S. Suslick, Y. Didenko, M. M. Fang, T. Hyeon, K. J. Kolbeck, W. B. McNamara III, M. M. Mdleleni, M. Wong, *Philos. Transact. A Math. Phys. Eng. Sci.* **1999**, *357*, 335–353.

[7] a) K. S. Suslick, E. B. Flint, *Nature* **1987**, *330*, 553–555; b) Y. T. Didenko, W. B. McNamara III, K. S. Suslick, *Nature* **2000**, *407*, 877–879.

[8] a) J. J. Kwan, R. Myers, C. M. Coviello, S. M. Graham, A. R. Shah, E. Stride, R. C. Carlisle, C. C. Coussios, *Small* **2015**, *11*, 5305–5314; b) U. Jonnalagadda, X. Su, J. Kwan, *Ultrason. Sonochem.* **2021**, *73*, 105530.

[9] U. S. Jonnalagadda, Q. Fan, X. Su, W. Liu, J. J. Kwan, *ChemCatChem* **2022**, *14*, e202200732.

[10] D. Han, D.-L. Zhou, Q.-Y. Guo, X. Lin, Q. Zhang, Q. Fu, *ACS Appl. Mater. Interfaces* **2021**, *13*, 31215–31225.

[11] Z. Xie, V. Mahendran, U. S. Jonnalagadda, Q. Fan, X. Su, A. F. Fischer, M. Tan, L. Tao, F. Jérôme, J. J. Kwan, S. Valange, T. S. Choksi, P. N. Amaniampong, W. Liu, *Green Chem., Advance article*, **2024**, DOI: 10.1039/D4GC03775H.

[12] a) Y. Duan, X. Liu, L. Han, S. Asahina, D. Xu, Y. Cao, Y. Yao, S. Che, *J. Am. Chem. Soc.* **2014**, *136*, 7193–7196; b) X. Sun, D. Wu, W. Zhu, X. Chen, R. Sharma, J. C. Yang, G. Zhou, *J. Phys. Chem. Lett.* **2021**, *12*, 9547–9556.

[13] a) R. Vasquez, *Surf. Sci. Spectra* **1998**, *5*, 262–266; b) D. Barreca, A. Gasparotto, E. Tondello, *Surf. Sci. Spectra* **2007**, *14*, 41–51.

[14] T. Bahry, S. Jiang, U. Jonnalagadda, W. Liu, B. Teychene, F. Jerome, S. H. Mushrif, P. N. Amaniampong, *Catal. Sci. Technol.* **2023**, *13*, 2982–2993.

[15] Q. T. Trinh, K. Bhola, P. N. Amaniampong, F. Jérôme, S. H. Mushrif, *J. Phys. Chem. C* **2018**, *122*, 22397–22406.

[16] a) Q. Zheng, D. Durben, G. Wolf, C. Angell, *Science* **1991**, *254*, 829–832; b) F. Caupin, E. Herbert, *C. R. Phys.* **2006**, *7*, 1000–1017.

[17] a) G. Kresse, J. Hafner, *Phys. Rev. B* **1993**, *47*, 558–561; b) G. Kresse, J. Furthmüller, *Comput. Mater. Sci.* **1996**, *6*, 15–50.

[18] Y. Guo, R. Hu, X. Zhou, J. Yu, L. Wang, *Appl. Surf. Sci.* **2019**, *479*, 989–996.

[19] C. M. Lousada, T. Brinck, M. Jonsson, *Comput. Theor. Chem.* **2015**, *1070*, 108–116.

[20] C. Michel, F. Auneau, F. Delbecq, P. Sautet, *ACS Catal.* **2011**, *1*, 1430–1440.
[21] a) P. N. Amaniampong, Q. T. Trinh, J. J. Varghese, R. Behling, S. Valange, S. H. Mushrif, F. Jérôme, *Green Chem.* **2018**, *20*, 2730–2741; b) K. Bhola, Q. T. Trinh, D. Liu, Y. Liu, S. H. Mushrif, *Catal. Sci. Technol.* **2023**, *13*, 6764–6779.
[22] a) P. N. Amaniampong, Q. T. Trinh, B. Wang, A. Borgna, Y. Yang, S. H. Mushrif, *Angew. Chem. Int. Ed.* **2015**, *54*, 8928–8933; b) R. Singuru, Q. T. Trinh, B. Banerjee, B. Govinda Rao, L. Bai, A. Bhaumik, B. M. Reddy, H. Hirao, J. Mondal, *ACS Omega* **2016**, *1*, 1121–1138.
[23] a) S. Xie, P. Huang, J. J. Kruzic, X. Zeng, H. Qian, *Sci. Rep.* **2016**, *6*, 21947; b) F. Lughmani, F. Nazir, S. A. Khan, M. Iqbal, *Cellulose* **2022**, *29*, 1911–1928; c) X. Sun, D. Xu, P. Dai, X. Liu, F. Tan, Q. Guo, *Chem. Eng. J.* **2020**, *402*, 125881.
[24] a) H. Lee, Y.-K. Park, S.-J. Kim, B.-H. Kim, H.-S. Yoon, S.-C. Jung, *J. Ind. Eng. Chem.* **2016**, *35*, 205–210; b) Q. T. Trinh, T. Le Van, T. T. N. Phan, K. P. Ong, H. Kosslick, P. N. Amaniampong, M. B. Sullivan, H.-S. Chu, H. An, T.-K. Nguyen, J. Zhang, J. Zhang, P. T. Huyen, N.-T. Nguyen, *J. Alloys Compd.* **2024**, *1002*, 175322.
[25] P. N. Amaniampong, Q. T. Trinh, T. Bahry, J. Zhang, F. Jérôme, *Green Chem.* **2022**, *24*, 4800–4811.

Manuscript received: August 28, 2024
Accepted manuscript online: October 14, 2024
Version of record online: ■■, ■■

Research Article

Catalysis by Cavitation Bubbles on CuO

V. Mahendran, Q. T. Trinh, X. Zhangyue, U. Jonnalagadda, T. Gould, N.-T. Nguyen, J. Kwan, T. S. Choksi, W. Liu, S. Valange, F. Jérôme, P. N. Amaniampong* e202416543

Localized Oxidative Catalytic Reactions Triggered by Cavitation Bubbles Confinement on Copper Oxide Microstructured Particles.

Localised oxidative catalytic reactions triggered by cavitation bubbles confinement on copper oxide microstructured particles.We exploit here a concept of CuO particle design with multiple gas-stabilizing sites, engineered to function as cavitation nuclei and catalysts. This concept facilitates selective and localised acoustic energy transfer directly to the catalyst surface, minimising the undesired dissipation of acoustic energy into the bulk solution while demonstrating superior cavitation properties at lower acoustic pressure amplitudes towards catalytic oxidative reactions.